RSC Advances

PAPER

View Article Online
View Journal | View Issue

Cite this: *RSC Adv.*, 2018, **8**, 39362

Adsorption separation of CO from syngas with CuCl@AC adsorbent by a VPSA process

Fei Gao,[a] Shougui Wang,[b] Weiwen Wang,[a] Jihai Duan,[a] Jipeng Dong[a] and Guanghui Chen *[a]

Received 16th October 2018
Accepted 20th November 2018

DOI: 10.1039/c8ra08578a

rsc.li/rsc-advances

In this work, activated carbon (AC) supported CuCl (CuCl@AC) prepared with $CuCl_2$ as precursor is investigated for CO separation from the synthesis gas mixture. Firstly, the CuCl@AC adsorbents are investigated for their CO reversible adsorption capacity at an operation temperature of 303 K. And a vacuum pressure swing adsorption (VPSA) process of CO separation from syngas utilizing the prepared CuCl@AC adsorbent is investigated at ambient temperature and 0.79 MPa through a dynamic optimization with Aspen Adsorption software. The integrated model is closer to a realistic PSA process, making the results of the simulation and optimization more convincing. The adsorption result reveals that the obtained CuCl@AC adsorbent with the copper loading of 7 mmol g^{-1} AC achieves a high reversible CO adsorption capacity and adsorption selectivity. The simulation result shows that, under optimal conditions, the CO product with the purity of 98.1 vol% can be separated from the syngas with the CO concentration of 32.3 vol% utilizing the prepared CuCl@AC adsorbent, and the recovery of CO is 92.9%.

1 Introduction

Carbon monoxide is an important chemical used widely as a raw material for the production of various chemicals including methanol, ethylene glycol, formic acid, acetic acid, polyurethane foams, polycarbonate plastics, *etc.*[1] The production of CO mainly utilizes the methods of the steam reforming of natural gas and coal gasification, producing a synthesis gas mixture containing CO, CO_2, CH_4, N_2 and H_2.[2] And then the high purity CO must be separated from the gas mixture for the production of various chemicals. In addition, huge amounts of CO are released from the tail gases of some industrial oxidation processes, such as coke oven gas, blast furnace gas, carbon black manufacturing tail gas, *etc.*[3–5] The CO from these tail gases should be separated and used from both the industrial and environmental point of views.

Recently, extensive efforts have been devoted to develop the technologies for CO separation from gas mixtures, including cryogenic distillation, liquid absorption and adsorption processes.[6] Cryogenic distillation is an extremely cost- and energy-intensive process, and suitable only when the CO-containing gas stream has a relatively low concentration of N_2 due to the similar boiling points.[7,8] Liquid absorption processes of CO utilizing ammoniacal cuprous chloride and aromatic $CuAlCl_4$ solution (COSORB) have the disadvantage of the instability of Cu^+ ions, which always react to give Cu^0 and Cu^{2+}.[9,10] Among these technologies, adsorptive separation like the pressure swing adsorption (PSA) appears to be the most promising and energy-saving alternative due to low energy costs and easy operations.[11,12]

For the adsorptive separation, CO adsorbents are the key to directly determine the separation performance.[13] In the development of adsorption separation technologies, various porous solids including activated carbon,[14,15] zeolites,[16,17] and metal–organic frameworks (MOFs)[18,19] display the high CO adsorption capacity. However, these adsorbents do not have significant adsorption selectivity for CO. Recently, CO separation[20–27] based on the Cu(I) π-complexation adsorbents could achieve high adsorption capacity and high adsorption selectivity for CO, resulting from the stronger π-complexation interactions of CO with Cu^+ ions supported on the porous solid materials. On the other hand, these types of bonds are still sufficiently weak to be broken by using simple engineering operations. Presently, the Cu(I)-based adsorbents are mainly prepared by dispersing CuCl onto the porous supports of zeolites or activated carbon (AC) using different dispersion methods. For the zeolites supported CuCl (CuCl@zeolites) adsorbents, the interactions of CO with CuCl@zeolites are relatively stronger than CuCl@AC resulting in a higher desorption temperature of ~453 K.[28] In the previous work of the first author involved in Tianjin University,[29] the activated carbon (AC) supported CuCl (CuCl@AC) adsorbent was successfully prepared with $CuCl_2$ as precursor by a solid-state dispersion method, and the activation of $CuCl_2$ supported on AC to CuCl was realized at 543 K in N_2 without any reducing gas. The prepared CuCl@AC adsorbent displayed high

[a]College of Chemical Engineering, Qingdao University of Science and Technology, Qingdao 266042, China. E-mail: guanghui@qust.edu.cn; Fax: +86 532 84022957; Tel: +86 532 84022957

[b]Fundamental Chemistry Experiment Center, Qingdao University of Science and Technology (Gaomi), Gaomi 261500, China

CO adsorption capacity and adsorption selectivity, and the adsorbed CO on CuCl@AC could be desorbed at lower temperature of 303 K under vacuum. This lower desorption temperature can greatly reduce the operation costs in CO separation processes compared with the higher desorption temperature of CuCl@zeolites. Thus, this CuCl@AC adsorbent has broad prospects for separation of CO from the synthesis gas mixture. So it is necessary to investigate the vacuum pressure swing adsorption (VPSA) process of CO separation from syngas utilizing CuCl@AC for designing a realistic PSA process.

In this work, a five-bed and 7-step VPSA process at ambient temperature of CO separation from syngas utilizing the prepared CuCl@AC adsorbent was investigated with Aspen Adsorption software. The operating conditions were optimized to obtain the high CO recovery and CO product purity. After optimization, the PSA process was analyzed, and the influence of the parameters on the process was explained.

2 Experimental

The CuCl@AC adsorbent with copper loadings of 7 mmol g^{-1} AC was prepared with $CuCl_2$ as precursor by a solid-state dispersion method according to the previous work of the first author involved in Tianjin University,[29] and denoted as CuCl(7.0)@AC. For an ideal adsorbent for gas separation in industrial application, it is required to be reversible for multiple adsorption and desorption cycles, and the adsorption and desorption cycle operations should be carried out at the same temperature. In the previous work,[29] the effect of the operation temperature on the reversible adsorption capacity of CO on CuCl@AC was investigated, and the optimum operation temperature was determined as 303 K. So, in this work, the reversible adsorptions of CO, CO_2, CH_4, N_2 and H_2 on CuCl(7.0)@AC at operation temperature of 303 K were measured using a static volumetric method[30,31] for investigating the PSA process. After adsorption of CO on CuCl(7.0)@AC, the desorption was carried out *in situ* by venting off the gas, vacuuming for 30 min with the mechanical vacuum pump at temperature of 303 K, and the adsorption equilibrium isotherms of CO, CO_2, CH_4, N_2 and H_2 on the desorbed adsorbents were measured again at the same temperature of 303 K, respectively.

3 Simulation of CO separation from syngas using a five-bed model

3.1 Process description

In this work, a five-bed and 7-step VPSA process at ambient temperature of CO separation from syngas utilizing the prepared CuCl@AC adsorbent was investigated with Aspen Adsorption software. Fig. 1 shows the flow diagram of this process, and the schedule is shown in Table 1. The relevant bed and adsorbent parameters used in the simulation are listed in Table 2, and the equilibrium and kinetic parameters for CO, CO_2, CH_4, N_2 and H_2 on CuCl@AC are listed in Tables 2 and 3. The overall process of each bed involves seven steps including adsorption (AD), pressure equalization for depressurization (ED), replacement (RP), blowdown (BD), vacuum (VU), pressure equalization for pressurization (EP) and feed repressurization (FR), and the total cycle time for the process is 20.0 min.[32,33] Take bed 1 for example, at the beginning of a cycle, the feed gas of syngas (32.3 vol% CO, 1.0 vol% CO_2, 2.4 vol% CH_4, 18.3 vol% N_2, 46.0 vol% H_2, $T = 303.15$ K, $p = 101.325$ kPa) passed through the adsorption bed after compression. During the adsorption step (AD), most of the CO from the mixture was selectively adsorbed on the CuCl@AC adsorbent, and the waste gas left from the adsorption bed. And at the first 60 s during the adsorption step, all the waste gas was introduced into pipe of gas waste. For the next 180 s during the adsorption step, one stream of the waste gas was drawn into the adsorption bed 2 to pressurize bed 2 in preparation for the adsorption. After the adsorption step, the ED step was conducted, and the gas of the bed 1 was introduced into bed 3 which was performing the EP step. Following the ED step, the replacement step (RP) was conducted utilizing part of the CO product to increase the concentration of CO and exclude the exhaust gas. And then the blowdown (BD) and vacuum (VU) steps were conducted to

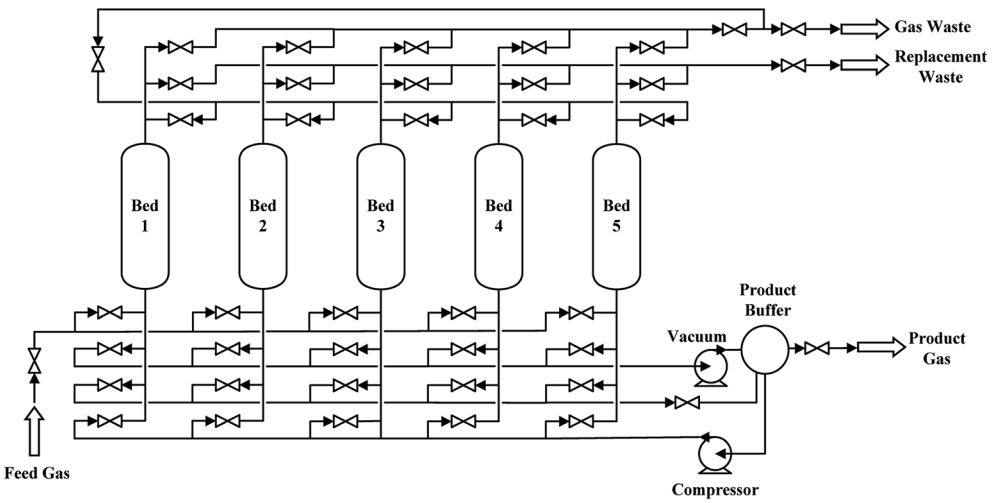

Fig. 1 Schematic flow diagram of five-bed VPSA process.

Table 1 Schedule of five-bed VPSA process

	60 s	180 s	60 s	180 s	60 s	180 s	60 s	180 s	60 s	180 s
Bed 1	AD↑	AD↑	ED↑	RP↑	RP↑	BD↓	VU↓	VU↓	EP↓	FR↓
Bed 2	EP↓	FR↓	AD↑	AD↑	ED↑	RP↑	RP↑	BD↓	VU↓	VU↓
Bed 3	VU↓	VU↓	EP↓	FR↓	AD↑	AD↑	ED↑	RP↑	RP↑	BD↓
Bed 4	RP↑	BD↓	VU↓	VU↓	EP↓	FR↓	AD↑	AD↑	ED↑	RP↑
Bed 5	ED↑	RP↑	RP↑	BD↓	VU↓	VU↓	EP↓	FR↓	AD↑	AD↑

regenerate the adsorbent and extract the high purity CO product. Finally, the EP and FR steps were conducted to increase the pressure of the bed for a new cycle.

3.2 Mathematical model

The following assumptions have been made for the mathematical models of the adsorption bed:[34–36] (i) the gas phase obey the ideal gas law; (ii) there are no radial variations in the temperature, pressure, and concentrations of gases in the solid and gas phase; (iii) gas flow can be described by the plug flow model; (iv) the kinetics of the adsorption are approximated by the LDF (linear driving force) model; (v) the void fractions in the bed and adsorbent were uniform.

Based on the above assumptions, the component and total mass balance with an estimated axial dispersion coefficient are established as follows:[37]

$$-\varepsilon_b D_{ax}\frac{\partial^2 c_i}{\partial z^2}+\frac{\partial(v_g c_i)}{\partial z}+\varepsilon_t\frac{\partial c_i}{\partial t}+j_i=0 \quad (1)$$

$$D_{ax}=0.73D_m+\frac{v_g R_p}{\varepsilon_b\left(1+9.49\frac{\varepsilon_b D_m}{2v_g R_p}\right)} \quad (2)$$

The LDF (linear driving force) model is defined by:[38]

$$j_i=\mathrm{MTC}_i(c_b-c_s)=-\rho_s\frac{\partial w_i}{\partial t} \quad (3)$$

The energy balance of the gas and solid phases are established in eqn (4)–(6).

$$-k_g\frac{\partial^2 T_g}{\partial z^2}+C_{vg}v_g\rho_g\frac{\partial T_g}{\partial z}+\varepsilon_b C_{vg}v_g\rho_g\frac{\partial T_g}{\partial t}+p\frac{\partial v_g}{\partial z}$$
$$+\mathrm{HTC}_{ap}(T_g-T_s)+\frac{4H_w}{D_B}(T_g-T_0)=0 \quad (4)$$

$$-k_s\frac{\partial^2 T_s}{\partial z^2}+\rho_s C_{ps}\frac{\partial T_s}{\partial t}+\rho_s\sum_{i=1}^{n}\left(C_{pa,i}w_i\right)\frac{\partial T_s}{\partial t}+\rho_s\sum_{i=1}^{n}\left(\Delta H_i\frac{\partial w_i}{\partial t}\right)$$
$$-\mathrm{HTC}_{ap}(T_g-T_s)=0 \quad (5)$$

$$-k_w\frac{\partial^2 T_w}{\partial z^2}+\rho_w C_{pw}\frac{\partial T_w}{\partial t}-H_w\frac{4D_B}{(D_B+W_T)^2-{D_B}^2}(T_g-T_w)$$
$$+H_{amb}\frac{4(D_B+W_T)^2}{(D_B+W_T)^2-{D_B}^2}(T_w-T_{amb})=0 \quad (6)$$

Table 2 Bed and adsorbent parameters used in the simulation

Parameters	Value	Units	Description
H_b	1.00	m	Height of bed
D_b	0.25	m	Internal diameter of bed
W_T	0.01	m	Wall thickness used of bed
ε_b	0.24	m^3 void/m^3 bed	Interparticle voidage
ε_p	0.21	m^3 void/m^3 bed	Intraparticle voidage
ρ_s	473	kg m^{-3}	Bulk solid density of adsorbent
R_p	0.001	m	Adsorbent particle radius
ψ	0.86	n/a	Adsorbent shape factor
MTC ("CH_4")	0.068	s^{-1}	Constant mass transfer coefficients
MTC ("CO")	0.17	s^{-1}	Constant mass transfer coefficients
MTC ("CO_2")	0.1	s^{-1}	Constant mass transfer coefficients
MTC ("H_2")	0.7	s^{-1}	Constant mass transfer coefficients
MTC ("N_2")	0.19	s^{-1}	Constant mass transfer coefficients
C_{ps}	0.857	kJ (kg K)$^{-1}$	Adsorbent specific heat capacity
C_{pw}	0.502	kJ (kg K)$^{-1}$	Heat capacity of wall
a_p	477	m^2 g^{-1}	Specific surface area of adsorbent
H_w	65	W (m^2 K)$^{-1}$	Heat transfer coefficient between wall and gas
k_g	0.242	W (m K)$^{-1}$	Heat conductivity of gas phase
k_s	0.3	W (m K)$^{-1}$	Heat conductivity of solid phase
k_w	17	W (m K)$^{-1}$	Heat conductivity of wall
ρ_w	7800	kg m^{-3}	Density of wall
T_{amb}	303.15	K	Ambient temperature

Table 3 Parameters of adsorption isotherm and physical parameters of adsorbates

Parameters	CH_4	CO	CO_2	H_2	N_2
IP_1/(kmol kg^{-1} bar^{-1})	1.79×10^{-4}	0.013	5.26×10^{-4}	4.52×10^{-5}	7.33×10^{-5}
IP_2/bar^{-1}	0.171	3.551	0.228	0.191	0.215
ΔH/(kJ mol^{-1})	−21.70	−31.40	−24.87	−11.84	−15.65
C_{pa}/(kJ kmol^{-1} K^{-1})	32.24	24.81	37.27	28.86	29.03

The pressure drop along the bed is calculated by the Ergun equation:

$$-\frac{\partial p}{\partial z} = \frac{1.5 \times 10^{-3}(1-\varepsilon_b)^2}{(2R_p\psi)^2 {\varepsilon_b}^3}\mu v_g + 1.75 \times 10^{-5} M \rho_g \frac{(1-\varepsilon_b)}{2R_p\psi {\varepsilon_b}^3} {v_g}^2 \quad (7)$$

Finally, the Langmuir model is used to describe the adsorption equilibrium isotherms of CO, CO_2, CH_4, N_2 and H_2 on the CuCl@AC adsorbent.

$$w_i = \frac{IP_{1i}p_i}{1 + \sum_k (IP_{2k}p_k)} \quad (8)$$

The PSA system is governed by the nonlinear equations listed in this section. In this work, the PDAEs were discretized in the spatial domain by a second-order central finite difference method with 50 axial nodes.[39]

4 Results and discussion

4.1 Adsorption isotherms of CO, CO_2, CH_4, N_2 and H_2

Fig. 2 gives the adsorption equilibrium isotherms of pure CO, CO_2, CH_4, N_2 and H_2 on the CuCl(7.0)@AC adsorbent at operation temperature of 303 K. Apparently, the adsorbent achieves a high reversible CO adsorption capacity, and can preferentially adsorb CO over CO_2, CH_4, N_2 and H_2, which is ascribed to the stronger interaction between the highly dispersed CuCl and CO *via* π-complexation and the weaker van der Waals and electrostatic interactions of CO_2, CH_4, N_2 and H_2 with the adsorbent.

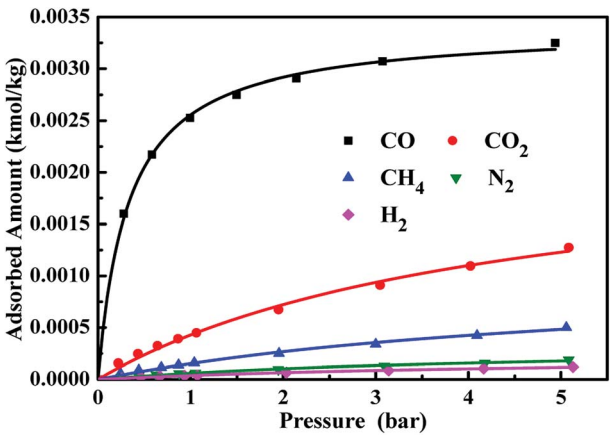

Fig. 2 Adsorption isotherms of CO, CO_2, CH_4, N_2 and H_2 on CuCl(7.0)@AC at operation temperature of 303 K.

In addition, the adsorption equilibrium isotherms were fitted by the Langmuir model, respectively, and fitting parameters are listed in Table 3.

4.2 Computational results

The simulation a five-bed VPSA process at ambient temperature of CO separation from syngas utilizing the prepared CuCl@AC adsorbent was conducted using Aspen Adsorption software with the adsorption isotherm parameters and the relevant adsorption bed parameters. The main objective is to analyze a medium-scale VPSA process and optimize the operating conditions. And the high CO purity of higher than 98 vol% and high CO recovery of higher than 90% are considered as the requirements of this VPSA process. The outlet flow rate of the waste gas and the replacement gas flow rate are the important parameters affecting the CO purity and CO recovery. Thus, in this work, these two parameters were optimized to achieve the required the CO purity and CO recovery. And the optimized result is listed in Table 4. Under the feed gas treatment amounts of 39.7 N m^3 h^{-1}, when the outlet flow rate of the waste gas and the replacement gas flow rate are 25.7 and 7.7 N m^3 h^{-1}, respectively, a high CO purity of 98.1 vol% with CO recovery of 92.9% is achieved, and outlet flow rate of the product gas is 12.1 N m^3 h^{-1}.

4.2.1 Pressure change of the five adsorption beds in a cycle.

Fig. 3 shows the pressure history curves of the five adsorption beds in a cycle. Take bed 1 for example to analyze the pressure change in this VPSA process. At the first 240 s, the compressed feed gas passes through the adsorption bed, and the pressure of bed 1 sharply increased to the required adsorption pressure of 0.79 MPa. After the adsorption (AD) step, the gas of the bed 1 was introduced into bed 3 to equalize pressure for 60 s, and the pressure decreased to 0.40 MPa. At the next 240 s, the replacement step (RP) was conducted utilizing CO product gas, and the pressure was kept at 0.41 MPa. And then the blowdown (BD) step was conducted for 180 s to vent the inside pressure for the next vacuum step, and the pressure decreased to 0.11 MPa.

Table 4 Concentrations of components in streams and the recovery of components in the product gas at a cycle steady state of the five-bed model

Components	CH_4	CO	CO_2	H_2	N_2
Product gas	0.2	98.1	0.3	0.9	0.5
Gas waste	3.3	2.8	1.2	66.5	26.2
Replacement waste	4.8	7.2	3.4	58.7	25.9
Recovery	2.2	92.9	9.0	0.6	0.8

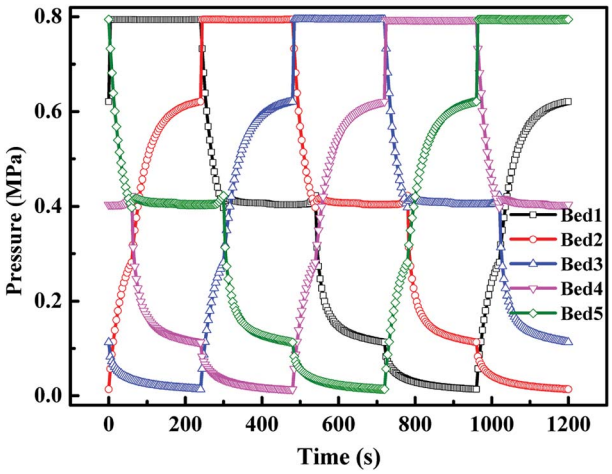

Fig. 3 Pressure history curves of five adsorption beds in a cycle.

Compared to the direct vacuum step, the conducted blowdown step can reduce the energy consumption. And then the vacuum (VU) step was conducted for 240 s to regenerate the adsorbent and extract the high purity CO product, and the pressure decreased to 0.014 MPa. A low vacuum level in the regeneration step is critical for good performance of the VPSA process. Finally, the pressure equalization for pressurization (EP) and feed repressurization (FR) steps were conducted to increase the pressure of the bed for a new cycle, and the pressure increased to 0.62 MPa.

4.2.2 Change of axial CO concentration on adsorption beds in a cycle. Fig. 4 shows the Change of axial CO concentration on adsorption bed 1 in a cycle. Seven measurement points are pinpointed among the adsorption bed with labeled Z/H for 0.00, 0.20, 0.40, 0.50, 0.60, 0.80 and 1.00, respectively, and $Z/H = 0.00$ is defined as the entrance of adsorption bed. It can be seen from Fig. 4 that, after the adsorption step, the adsorption bed at $Z/H = 0.00$–0.60 reached the saturation for the CO adsorption. During the ED step, some impurity gases were discharged from the adsorption bed, and the CO concentration increased slightly. During the replacement step, the CO concentration in adsorption bed increased gradually, and after the replacement step, the CO concentration in adsorption bed was higher than 98% except for the bed outlet, *i.e.*, at the end of the replacement step, the adsorption bed at $Z/H = 1.00$ just going to be saturated for the CO adsorption. Thus, the adsorbents were fully utilized at the optimal condition.

4.2.3 Axial concentration distribution in gas phase at the end of each step. Fig. 5 shows the axial concentration profiles of CO, CO_2, CH_4, N_2 and H_2 after the adsorption (AD) step. In can be seen that, after the adsorption step, the adsorption bed at $Z/H = 0.00$–0.60 reached the saturation, and the concentration of CO, CO_2, CH_4, N_2 and H_2 did not change with the axial distance of the bed, which consistent with the concentration of each component in feed gas. And in the unsaturated adsorption bed at $Z/H > 0.60$, with the increase of axial distance of the bed, CO concentration decreased gradually, and the concentration of other components increased gradually. Finally, the concentrations of all components tend to be stable.

Fig. 6 shows the axial concentration profiles of CO, CO_2, CH_4, N_2 and H_2 after the step of pressure equalization for depressurization (ED). During the ED step, the pressure was released to the adsorption bed which needs to be pressurized, and some impurity gases were discharged from the adsorption bed. Thus, compared with the adsorption step, at the end of ED step, the CO concentration increased, and the concentration of other components decreased. In addition, from Fig. 6, after the ED step, the axial distance of saturated adsorption bed moved from $Z/H = 0.6$ to 0.7. Fig. 7 shows the axial concentration profiles of CO, CO_2, CH_4, N_2 and H_2 after replacement (RP) step. The replacement step, also called the product purge step, aims to exclude impurity gases from the adsorption bed and increase the concentration of CO in the adsorption bed utilizing part of the CO product. The extent of replacement can greatly affect the purity and recovery of CO. It can be seen from Fig. 7 that, except for the outlet of adsorption bed, the CO concentration in adsorption bed was higher than 98% at the end of replacement step, and the concentration of other components was close to 0.

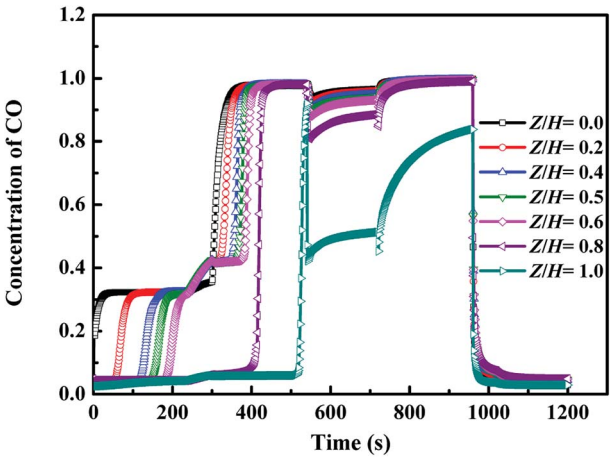

Fig. 4 Change of axial CO concentration on adsorption beds in a cycle (Z, axial distance of adsorption beds; H, height of adsorption bed).

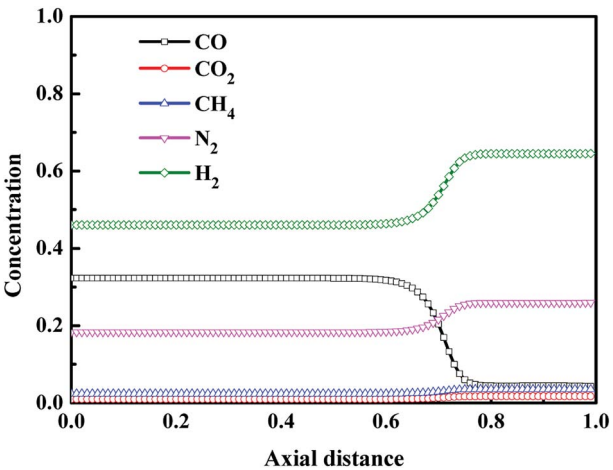

Fig. 5 Concentration profiles in gas phase after the adsorption step.

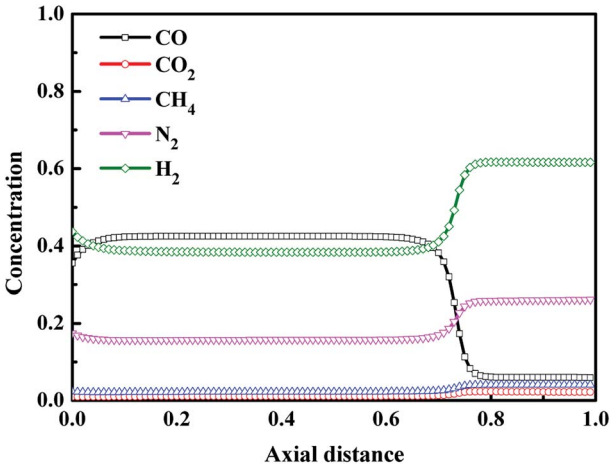

Fig. 6 Concentration profiles in gas phase after the step of pressure equalization for depressurization.

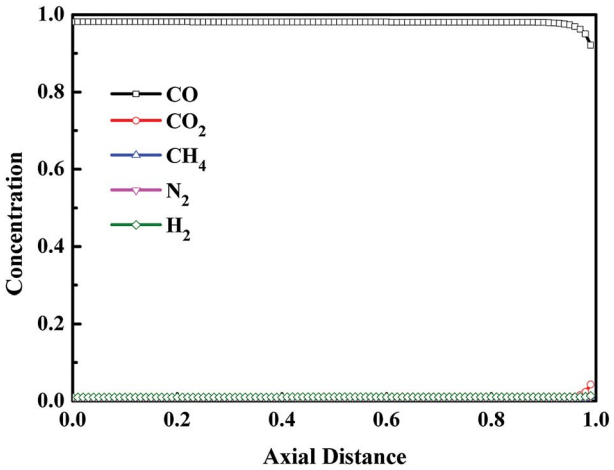

Fig. 7 Concentration profiles in gas phase after the replacement step.

The result indicates that the replacement process is sufficient at the optimal condition.

The axial concentration profiles in gas phase after the blowdown (BD) step and the vacuum (VU) step are depicted in Fig. 8 and Fig. 9, respectively. For VPSA processes, the evacuated pressure is one of the critical benefits to improve the recovery of the product. The blowdown and vacuum steps play the same role in VPSA processes. And unlike the vacuum step, the blowdown step does not consume any energy. After the blowdown step, the pressure of the adsorption bed decreased to 0.11 MPa. From the adsorption isotherms of CO, CO_2, CH_4, N_2 and H_2 on CuCl(7.0)@AC (see Fig. 1), it can be seen that, during the blowdown step, most of the light component gas adsorbed on the adsorption bed was desorbed from the adsorbents, while only a small amount of adsorbed CO was desorbed. Thus, compared with replacement step, after the blowdown step, the concentration of light components increased, and the CO concentration decreased. In addition, it can be seen from Fig. 8 that the impurity gases were mainly concentrated on the top of the adsorption bed. During the vacuum step, the pressure of the

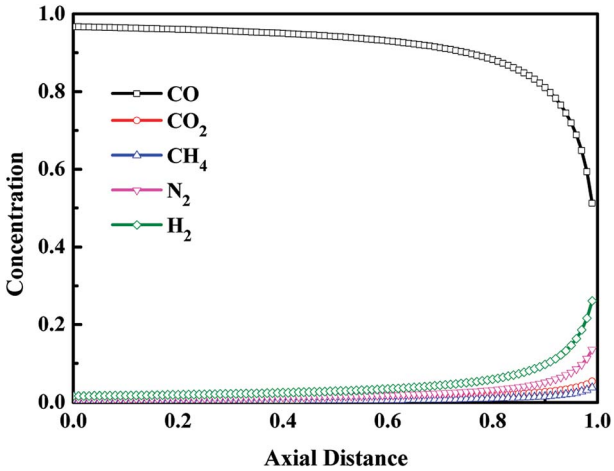

Fig. 8 Concentration profiles in gas phase after the blowdown step.

adsorption bed further decreased to 0.014 MPa, and the adsorbed CO was almost completely desorbed from the adsorption bed and introduced to the product gas system. And

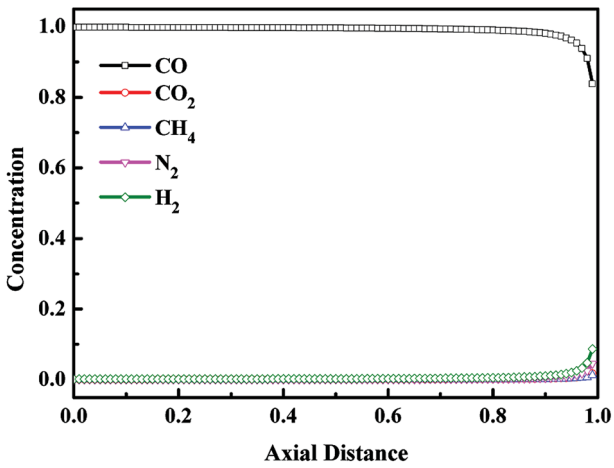

Fig. 9 Concentration profiles in gas phase after the vacuum step.

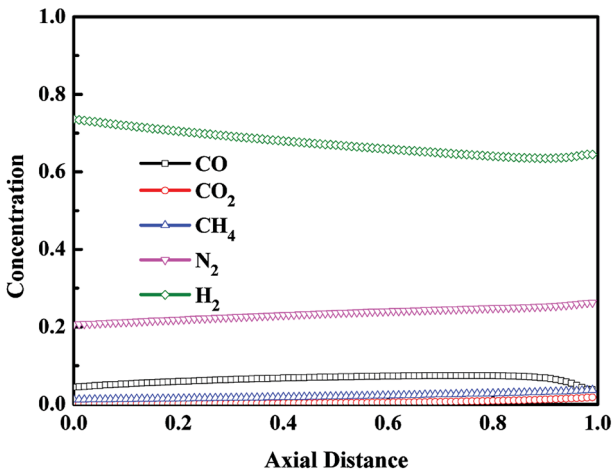

Fig. 10 Concentration profiles in gas phase after the step of pressure equalization for pressurization.

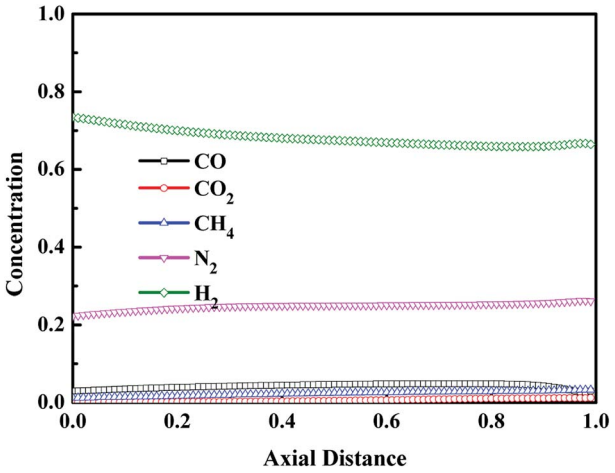

Fig. 11 Concentration profiles in gas phase after the feed repressurization step.

it can be seen from Fig. 9 that, except for the outlet of adsorption bed, the CO concentration in adsorption bed was higher than 99% at the end of vacuum step, and the concentration of other components was close to 0.

Fig. 10 and 11 display the axial concentration distributions in gas phase after the step of pressure equalization for pressurization (EP) and the step of the feed repressurization (FR), respectively. These two steps were conducted to increase the pressure of the bed for a new cycle utilizing the pressurized gas from the beds performing the step of pressure equalization for depressurization and the step of adsorption, respectively, in which the CO concentration was at a low level, and the concentration of other components was high. Thus, at the optimal condition, the CO concentration of the bed was maintained at a low level after these two steps.

5 Conclusions

In this work, the activated carbon (AC) supported CuCl (CuCl@AC) is investigated for CO separation from the synthesis gas mixture. This CuCl/AC adsorbent achieves a high reversible CO adsorption capacity at lower operation temperature of 303 K. A simulation and optimization of five-bed VPSA for the CO separation from syngas on CuCl@AC has been described and discussed. The operation step of adsorbent beds in this process is governed by valves and dynamic boundaries that are close to realistic conditions. The operating conditions have been optimized for maximizing the CO recovery and CO product purity by adjusting the outlet flow rate of the waste gas and the replacement gas flow rate. The optimization result indicate that the performance of the VPSA process can be improved under the operating restrictions, and a significantly high recovery (92.9%) and purity (98.1 vol%) of CO can be achieved from the syngas with a low CO concentration (32.3 vol%). This VPSA process is operated at ambient temperature, which can great reduce the operation costs in CO separation processes. In addition, the systematic analysis of this VPSA process can provide significant insight for designing a realistic PSA process.

Conflicts of interest

There are no conflicts to declare.

Nomenclature

c_i	Gas phase concentration of component i (mol m^{-3})
C_{vg}	Heat capacity of the gas at constant volume (kJ kmol^{-1} K^{-1})
C_{ps}	Adsorbent specific heat capacity (kJ kg^{-1} K^{-1})
C_{pa}	Heat capacity of the gas at constant pressure (kJ kmol^{-1} K^{-1})
D_{ax}	Axial dispersion coefficient (m^2 s^{-1})
D_m	Molecular diffusivity coefficient (m^2 s^{-1})
D_b	Internal diameter of bed (m)
H_w	Heat transfer coefficient between wall and gas (W m^{-2} K^{-1})
H_b	Height of bed (m)
IP_1	Adsorption equilibrium constant (bar^{-1})
IP_2	Adsorption equilibrium constant (kmol kg^{-1} bar^{-1})
MTC_i	Constant mass transfer coefficients (s^{-1})
M	Molecular weight (kg mol^{-1})
k_g	Heat conductivity of gas phase (W m^{-1} K^{-1})
k_s	Heat conductivity of solid phase (W m^{-1} K^{-1})
k_w	Heat conductivity of wall (W m^{-1} K^{-1})
p_i	Pressure (bar)
R	Gas constant (J mol^{-1} K^{-1})
R_p	Adsorbent particle radius (m)
T_{amb}	Ambient temperature (K)
T_g	Temperature of gas phase (K)
T_s	Temperature of solid phase (K)
T_0	Temperature of wall (K)
v_g	Gas velocity (m s^{-1})
W_T	Wall thickness (m)
y_i	Mole fraction of component i
ε_b	Bed void fraction
ε_p	Particle void fraction
ρ_s	Particle density (kg m^{-3})
ψ	Shape factor
μ	Gas viscosity (kg m^{-1} s^{-1})
ΔH	Isosteric heat of adsorption of component (kJ mol^{-1})

Acknowledgements

This work has been supported by Natural Science Foundation of Shandong Province (No. ZR2018BB071) and a Project of Shandong Province Higher Educational Science and Technology Program (No. J17KA107).

Notes and references

1 D. Saha and S. Deng, Adsorption equilibria and kinetics of carbon monoxide on zeolite 5A, 13X, MOF-5, and MOF-177, *J. Chem. Eng. Data*, 2009, **54**, 2245–2250.
2 N. Heymans, B. Alban, S. Moreau and G. De Weireld, Experimental and theoretical study of the adsorption of

pure molecules and binary systems containing methane, carbon monoxide, carbon dioxide and nitrogen. Application to the syngas generation, *Chem. Eng. Sci.*, 2011, **66**, 3850–3858.

3 T. Harlacher, T. Melin and M. Wessling, Techno-economic analysis of membrane-based argon recovery in a silicon carbide process, *Ind. Eng. Chem. Res.*, 2013, **52**, 10460–10466.

4 T. Harlacher, M. Scholz, T. Melin and M. Wessling, Optimizing argon recovery: membrane separation of carbon monoxide at high concentrations *via* the water gas shift, *Ind. Eng. Chem. Res.*, 2012, **51**, 12463–12470.

5 G. Zarca, I. Ortiz and A. Urtiaga, Kinetics of the carbon monoxide reactive uptake by an imidazolium chlorocuprate(I) ionic liquid, *Chem. Eng. J.*, 2014, **252**, 298–304.

6 G. Zarca, I. Ortiz and A. Urtiaga, Copper(I)-containing supported ionic liquid membranes for carbon monoxide/nitrogen separation, *J. Membr. Sci.*, 2013, **438**, 38–45.

7 G. S. Patil, S. Baruah and N. N. Dutta, Facilitated transport of carbon monoxide: a review, *Gas Sep. Purif.*, 1991, **5**, 2–8.

8 F. Kasuya and T. Tsuji, High purity CO gas separation by pressure swing adsorption, *Gas Sep. Purif.*, 1991, **5**, 242–246.

9 D. J. Safarik and R. B. Eldridge, Olefin/paraffin separations by reactive absorption: a review, *Ind. Eng. Chem. Res.*, 1998, **37**, 2571–2581.

10 J. A. Hogendoorn, W. P. M. van Swaaij and G. F. Versteeg, The absorption of carbon monoxide in COSORB solutions: absorption rate and capacity, *Chem. Eng. J.*, 1995, **59**, 243–252.

11 R. T. Yang, *Adsorbents: Fundamentals and Applications*, Wiley, New York, 2003.

12 N. N. Dutta and G. S. Patil, Developments in CO separation, *Gas Sep. Purif.*, 1995, **9**, 277–283.

13 L. Wang, J. Zhao, L. Wang, T. Yan, Y.-Y. Sun and S. B. Zhang, Titanium-decorated graphene oxide for carbon monoxide capture and separation, *Phys. Chem. Chem. Phys.*, 2011, **13**, 21126–21131.

14 J. A. Delgado, V. I. Águeda, M. A. Uguina, J. L. Sotelo, P. Brea and C. A. Grande, Adsorption and diffusion of H_2, CO, CH_4, and CO_2 in BPL activated carbon and 13X zeolite: evaluation of performance in pressure swing adsorption hydrogen purification by simulation, *Ind. Eng. Chem. Res.*, 2014, **53**, 15414–15426.

15 F. V. S. Lopes, C. A. Grande, A. M. Ribeiro, J. M. Loureiro, O. Evaggelos, V. Nikolakis and A. E. Rodrigues, Adsorption of H_2, CO_2, CH_4, CO, N_2 and H_2O in activated carbon and zeolite for hydrogen production, *Sep. Sci. Technol.*, 2009, **44**, 1045–1073.

16 H. Tsutaya and J. Lzumi, Carbon monoxide adsorption by zeolite, *Zeolites*, 1991, **11**, 90.

17 G. Sethia, R. S. Somani and H. Chand Bajaj, Adsorption of carbon monoxide, methane and nitrogen on alkaline earth metal ion exchanged zeolite-X: structure, cation position and adsorption relationship, *RSC Adv.*, 2015, **5**, 12773–12781.

18 V. I. Agueda, J. A. Delgado, M. A. Uguina, P. Brea, A. I. Spjelkavik, R. Blom and C. Grande, Adsorption and diffusion of H_2, N_2, CO, CH_4 and CO_2 in UTSA-16 metal-organic framework extrudates, *Chem. Eng. Sci.*, 2015, **124**, 159–169.

19 K. Munusamy, G. Sethia, D. V. Patil, P. B. Somayajulu Rallapalli, R. S. Somani and H. C. Bajaj, Sorption of carbon dioxide, methane, nitrogen and carbon monoxide on MIL-101(Cr): volumetric measurements and dynamic adsorption studies, *Chem. Eng. J.*, 2012, **195–196**, 359–368.

20 C. J. King, in *Handbook of Separation Process Technology*, ed. R. W. Rousseau, Wiley, New York, 1987.

21 T. C. Golden, W. C. Kratz, F. C. Wilhelm, R. Pierantozzi and A. Rokicki, Highly dispersed cuprous compositions, *US Pat.*, 5.175.137, 1992.

22 H. Hirai, K. Wada and M. Komiyama, Active carbon-supported copper(I) chloride as solid adsorbent for carbon monoxide, *Bull. Chem. Soc. Jpn.*, 1986, **59**, 2217–2223.

23 H. Hirai, K. Wada, K. Kurima and M. Komiyama, Carbon monoxide adsorbent composed of copper(I) chloride and polystyrene resin having amino groups, *Bull. Chem. Soc. Jpn.*, 1986, **59**, 2553–2558.

24 H. Tamon, K. Kitamura and M. Okazaki, Adsorption of carbon monoxide on activated carbon impregnated with metal halide, *AIChE J.*, 1996, **42**, 422–430.

25 Y. Xie, J. Zhang, J. Qiu, X. Tong, J. Fu, G. Yang, H. Yan and Y. Tang, Zeolites modified by CuCl for separating CO from gas mixtures containing CO_2, *Adsorption*, 1997, **3**, 27–32.

26 J. Ma, L. Li, J. Ren and R. Li, CO adsorption on activated carbon-supported Cu-based adsorbent prepared by a facile route, *Sep. Purif. Technol.*, 2010, **76**, 89–93.

27 J. Peng, S. Xian, J. Xiao, Y. Huang, Q. Xia, H. Wang and Z. Li, A supported Cu(I)@MIL-100(Fe) adsorbent with high CO adsorption capacity and CO/N_2 selectivity, *Chem. Eng. J.*, 2015, **270**, 282–289.

28 F. Gao, Y. Wang and S. Wang, Selective adsorption of CO on CuCl/Y adsorbent prepared using $CuCl_2$ as precursor: equilibrium and thermodynamics, *Chem. Eng. J.*, 2016, **290**, 418–427.

29 F. Gao, Y. Wang, X. Wang and S. Wang, Selective CO adsorbent CuCl/AC prepared using $CuCl_2$ as a precursor by a facile method, *RSC Adv.*, 2016, **6**, 34439–34446.

30 Z. Huang, L. Xu, J. Li, G. Guo and Y. Wang, Adsorption equilibrium of carbon dioxide and methane on β-zeolite at pressures of up to 2000 kPa using a static volumetric method, *J. Chem. Eng. Data*, 2010, **55**, 2123–2127.

31 M. Delavar, A. A. Ghoreyshi, M. Jahanshahi, S. Khalili and N. Nabian, Equilibria and kinetics of natural gas adsorption on multi-walled carbon nanotube material, *RSC Adv.*, 2012, **2**, 4490–4497.

32 S. P. Reynolds, A. Mehrotra, A. D. Ebner and J. A. Ritter, Heavy reflux PSA cycles for CO_2 recovery from flue gas: Part I. Performance evaluation, *Adsorption*, 2008, **14**, 399–413.

33 Z. Liu, C. A. Grande, P. Li, J. Yu and A. E. Rodrigues, Multi-bed vacuum pressure swing adsorption for carbon dioxide capture from flue gas, *Sep. Purif. Technol.*, 2011, **81**, 307–317.

34 C. T. Chou and W. C. Huang, Simulation of a four bed pressure swing adsorption process for oxygen enrichment, *Ind. Eng. Chem. Res.*, 1994, **33**, 1250–1258.

35 C. Z. Shen, Z. Liu, P. Li and J. Yu, Two-stage VPSA process for CO_2 capture from flue gas using activated carbon beads, *Ind. Eng. Chem. Res.*, 2012, **51**, 5011–5021.
36 H. Yang, C. Yin, B. Jiang and D. Zhang, Optimization and analysis of a VPSA process for N_2/CH_4 separation, *Sep. Purif. Technol.*, 2015, **134**, 232–240.
37 R. T. Yang, *Gas Separation by Adsorption Process*, Butterworths, Boston, 1987, pp. 50–101.
38 A. Olajossy, A. Gawdzik, Z. Budner and J. Dula, Methane separation from coal mine methane gas by vacuum pressure swing adsorption, *Chem. Eng. Res. Des.*, 2003, **81**, 474–482.
39 R. Haghpanah, A. Majumder, R. Nilam, A. Rajendran, S. Farooq, I. A. Karimi and M. Amanullah, Multiobjective optimization of a four-step adsorption process for postcombustion CO_2 capture *via* finite volume simulation, *Ind. Eng. Chem. Res.*, 2013, **52**, 4249–4265.